A Compact Dual-band MIMO Antenna for 5G Mobile Communications

Jianxun Su, Zhengyu Dai, Jianhe Du *, Jiayong Yu, Zeqiang Chen, and Zengrui Li *

School of Information and Engineering
Communication University of China, Beijing, 100024, China
sujianxun_jlgx@163.com, zrli@cuc.edu.cn*, dujianhe1@gmail.com*

Abstract ─ In this paper we propose a compact dual-band MIMO antenna for 5G mobile communications. Its element is a dual-band monopole working at 3.4 GHz and 4.9 GHz. In order to cover the commercial 5G communication band of sub-6 GHz (3.3-3.6 GHz and 4.8-5.0 GHz), an inverted L-shaped strip is added on the ground of the monopole to achieve a band-notch of S_{11} at 3.4 GHz and a quasi-directional radiation pattern. The proposed MIMO antenna has a compact size of 50*50*0.8mm^3 and it's composed of four improved monopoles mentioned above with mutually orthogonal placement. Long strips are loaded on the ground layer and antenna layer to obtain a better port isolation at 3.3-3.6 GHz. The measured results show that the reflection coefficient (S_{ii}) of the MIMO antenna is less than -10 dB at the lower band and less than -20dB at the higher band. Its -10dB-bandwidth covers the band of 3.3-5.8 GHz and the mutual coupling (S_{ij}) between ports keeps lower than -20dB within the dual-band. The envelope correlation coefficients (ECC) of the MIMO antenna are also measured and they're below 0.01. A channel model is used to calculate the MIMO channel capacity and the results show this MIMO channel performs best at 5 GHz.

Index Terms ─ Channel capacity, dual-band monopole antenna, envelope correlation coefficient (ECC), fifth generation (5G) communication, multiple-input-multiple-output (MIMO) antenna, mutual coupling.

I. INTRODUCTION

In the past decades, wireless communication technology has got rapid and unprecedented development. At the same time a lot of problems emerged as there were growing appetites for safer and faster data transmission. In addition, with the development and standards' building of the fifth-generation (5G) mobile communication, more and more researches have been carried into related technologies with the hope of higher transmission rate, lower cost and higher gain. Multiple-input-multiple-output (MIMO) technology is the key to realize a higher transmission rate.

By using MIMO technology, we can establish multiple independent channels on the original spectrum by diversity method and reduce multipath fading, so as to improve data transmission rate [1].

MIMO antenna is the significant facility to improve channel capacity of MIMO system. For traditional single-port antenna, the reflection coefficient (S_{ii}) is used to describe reflection loss of input; while for MIMO antenna, the mutual coupling (S_{ij}) is also important to indicate the energy from port-j to port-i. Strong mutual coupling will worsen the receiving/sending performance of MIMO antenna.

In order to suppress the mutual coupling, a lot of attempts have been tried to improve the isolation between ports in MIMO antenna [2-10]. Such as the defected ground structures (DGS) proposed in [3-4], decoupling network structures presented in [5-6] and electromagnetic band-gap (EBG) structures shown in [7-10]. Researches in [11-12] presented the applications of polarization diversity technology in MIMO communication system and its improvement of channel capacity in detail. By the way, many kinds of 5G MIMO antennas have been put forward in recent years [13-17].

In this paper, a compact dual-band 4-port MIMO antenna works within 3.3-3.6 GHz and 4.8-5.0 GHz (sub-6 GHz) is proposed. The MIMO antenna has a good performance and its measured results agree well with simulated results. In designs of many MIMO antennas, it's common to avoid placing elements in parallel and choose to place them vertically, which can avoid strong mutual couplings caused by the same polarization mode. However, in this paper the antenna elements are perpendicular to each other and parallel to each other. In addition, the MIMO antenna achieves not only low mutual couplings but also compact size.

The paper is organized as follows: the design of the antenna element and the final MIMO antenna are introduced in Section II. Section III discusses the measured and calculated results of the S-parameters, radiation patterns and channel capacity etc. Section IV gives a conclusion of this paper.

Submitted On: July 8, 2019
Accepted On: September 7, 2019

II. THE DUAL-BAND MIMO ANTENNA

A. Antenna element configuration

The MIMO antenna's element is an improved monopole and its structure is shown in Fig. 1 with the small size of 25*25*0.8mm^3. The upper layer is a circular monopole fed by microstrip line and they are printed on a FR4 substrate (permittivity=4.4±0.1 and loss tangent=0.02±0.001) [18]. Inspired from the isolation enhancement ability of the L-shaped strip used in [19-20], we use the L-shaped strip to acquire a dual-band monopole and configure the proposed 4-port MIMO antenna. The inverted L-shaped strip extending from the ground and the detailed dimensions of the improved monopole are shown in Fig. 1 and Table 1. The L-shaped strip works as a radiator at 3.4 GHz and a reflector at 4.9 GHz.

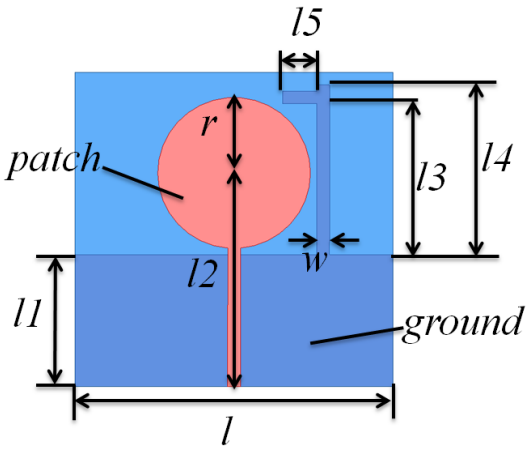

Fig. 1. Geometry of the improved monopole.

Table 1: Dimensions of the improved monopole

l	***l1***	***l2***	***l3***
25mm	10.5mm	17mm	12mm
l4	***l5***	***r***	***w***
13.5mm	2.7mm	6mm	1mm

The 3D radiation patterns and the S-parameters of the monopole with/without inverted L-shaped strip are shown in Fig. 2 and Fig. 3. The monopole without inverted L-shaped strip works at 5.45 GHz, and its radiation pattern is symmetrical. However, after adopting the inverted L-shaped strip on ground, S_{11} can achieve a band-notch at 3.4 GHz and its original resonance point of 5.45 GHz moves to 4.9 GHz. It's worth noting that the direction of maximum radiation steers to left side, which is important for the configuration of MIMO antenna in the next.

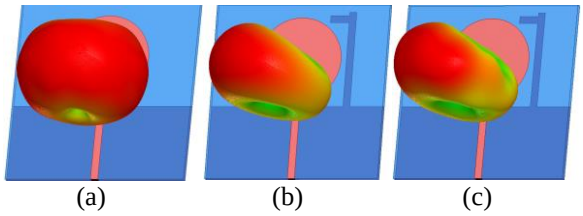

Fig. 2. 3D radiation patterns of the monopole: (a) without inverted L-shaped strip at 5.45 GHz, (b) with inverted L-shaped strip at 3.4 GHz, and (c) 4.9 GHz.

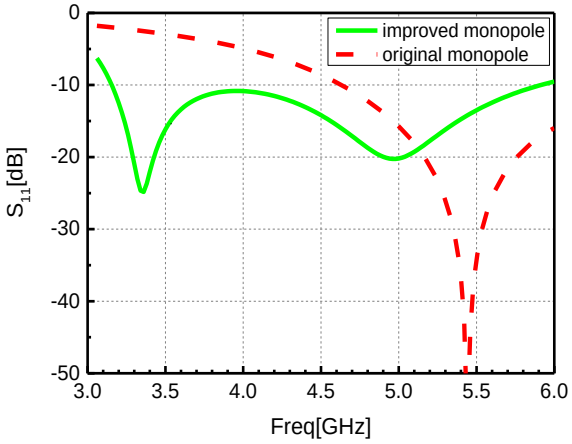

Fig. 3. S_{11} of improved monopole and original monopole.

In order to have a better illumination about the working mechanism of improved monopole, its simulated current distributions at 3.4 GHz and 4.9 GHz are shown in Fig. 4 respectively: when the antenna works at 4.9 GHz, the current is mainly distributed near the circular patch and the L-shaped strip acts as a reflector, which makes the maximum radiation direction shift to the left side; while at 3.4 GHz, the current can be coupled to the L-shaped strip from right side of the circular patch, which makes it act as a 0.4λ length radiator. And the L-shaped strip itself shows a left steering radiation pattern at 3.4 GHz due to the bending at the top.

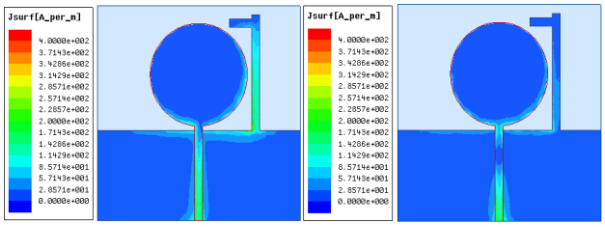

Fig. 4. Current distributions of the improved monopole antenna at: (a) 3.4 GHz and (b) 4.9 GHz.

B. Four-port MIMO antenna

Four improved monopoles mentioned above were placed in two orthogonal directions to form a four-port MIMO antenna with a size of 50*50*0.8mm^3. Its structure is shown in Fig. 5 (a). Figure 6 (a) shows the S-parameters of the antenna in Fig. 5 (a). It can be observed that isolations between ports (S_{21} & S_{41}) are close to 11 dB within 3.3-3.6 GHz. That's because the main radiation elements at 3.4 GHz are the L-shaped strips but they are spread too tightly on the ground, which results strong mutual couplings. In addition, within 4.8-5.0 GHz, mutual couplings are less than -20 dB.

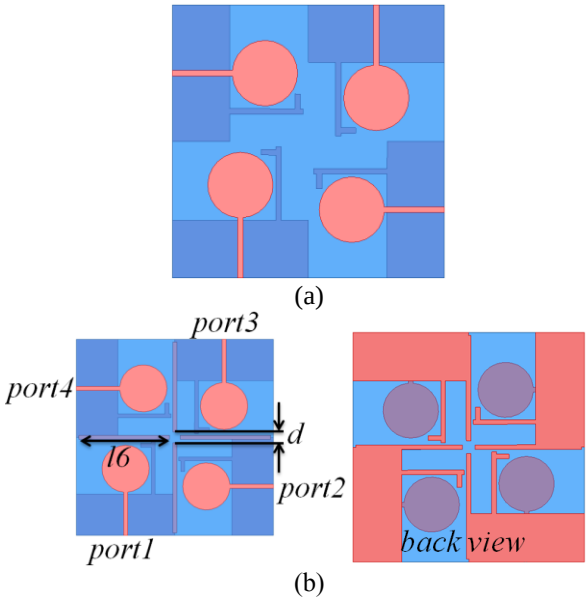

Fig. 5. Four-port MIMO antenna: (a) without long strips, and (b) with long strips (*l*6=23, *d*=2.7. unit: mm).

To reduce the mutual couplings within 3.3-3.6 GHz, we employ eight long strips with a length of 23mm (about 0.55λ at 3.5 GHz). As shown in Fig. 5 (b), four strips are loaded on antenna layer and another four are placed at the same place but on the ground layer. The L-shaped strips are located at the maximum radiation direction of adjacent elements, thus generating coupling energy to adjacent ports. Those long strips can work as a parasitic resonator to add the coupling path between elements and then reduce the mutual couplings. Figure 6 (b) shows the S-parameters of MIMO antenna shown in Fig. 5 (b). It can be inferred that the S_{21} & S_{41} are successfully reduced to -15 dB within 3.3-3.6 GHz, and its S_{11} is nearly unaffected.

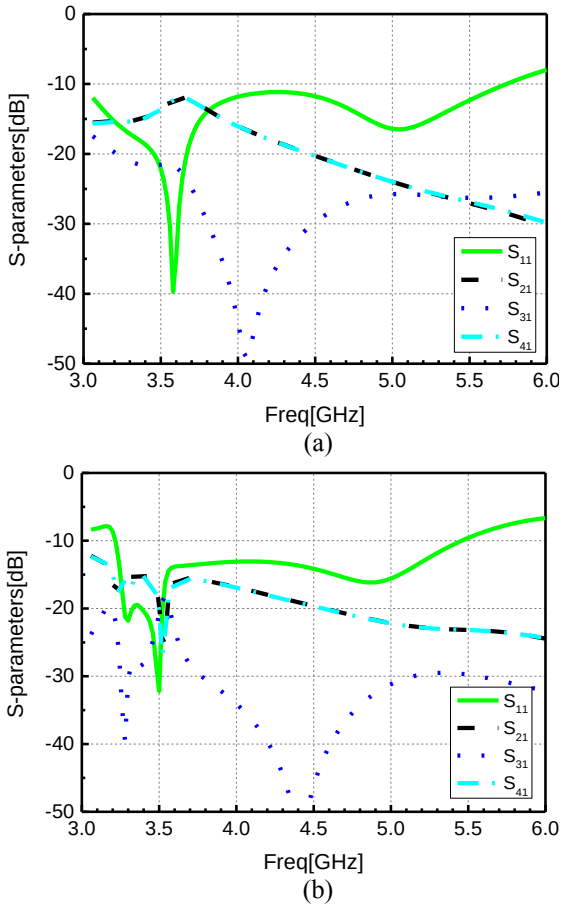

Fig. 6. Simulated S-parameters of MIMO antenna shown in Fig. 5: (a) without long strips, and (b) with long strips.

Figure 7 presents the simulated current distributions of the MIMO antenna without/with the long strips at 3.5 GHz and 4.9 GHz respectively, in which Port 1 is excited and other ports are terminated with a 50-Ω load. When the MIMO antenna without the long strips works at 3.4 GHz, there is strong current distributed near the L-shaped strips of port 2 and port 4, which leads to the high S_{21} and S_{41}, as shown in the simulated results of Fig. 6 (a). However, after loading these long strips on MIMO antenna the coupling current mostly distribute alone the strips, which can dramatically avoid the energy coupled from port1 to port2 & port4 directly and make S_{21} and S_{41} reduced consequently at 3.3-3.6 GHz. By the way, the mutual couplings between antenna elements are still less than -20 dB when the MIMO antenna works at 4.9 GHz.

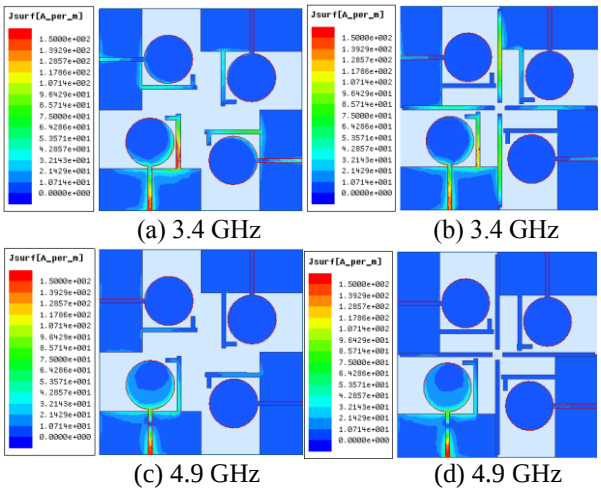

(a) 3.4 GHz (b) 3.4 GHz

(c) 4.9 GHz (d) 4.9 GHz

Fig. 7. Current distributions of the MIMO antenna without/with long strips at: (a)-(b) 3.4 GHz, and (c)-(d) 4.9 GHz.

III. RESULTS AND DISCUSSION

A. Experiment verification

In order to verify the simulated results mentioned above, the MIMO antenna was fabricated and measured. A vector network analyzer (Agilent PNA-L N5234A) was used to measure the antenna in our research. The fabricated MIMO antenna and the measured results of S-parameters are given in Fig. 8. As we know, the permittivity of FR4 varies a lot in practical application of microwave. Inferred from the analysis and measurement of [18], the measured resonance points of antenna based on FR4 are very close to the theoretical values within 2-8 GHz, but it varies a lot at higher frequencies like 10 GHz. So, in our measured results of 3-6 GHz, the change of FR4's properties have little impact.

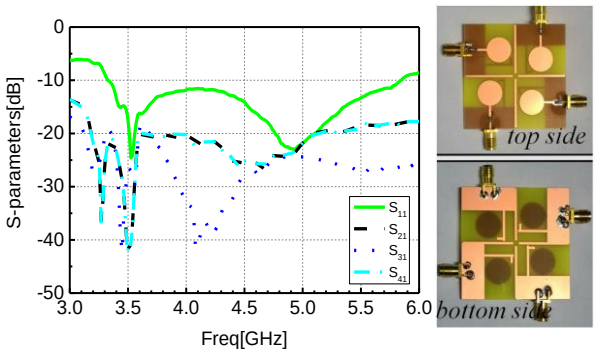

(a) (b)

Fig. 8. (a) Measured S-parameters of MIMO antenna, and (b) fabricated antenna's top side and bottom side.

In Fig. 8 (a), the MIMO antenna can cover the dual-band of sub-6 GHz: it provides a quite good impedance bandwidth (S_{11} < -10 dB within 3.3-3.6 GHz and S_{11} < -20 dB within 4.8-5.0 GHz), and its -10 dB-bandwidth can even cover 3.3-5.8 GHz. However, in the simulation we don't consider the connection of transmission line and welding of SMA connector, which may explain why the measured results of S_{11} are higher than simulation results at 3.3-3.6 GHz. Meanwhile, the mutual couplings between the ports keep low enough: the S_{ij} < -20 dB within the dual-band, that's because the measured results of S_{11} are higher than simulated results (more energy are reflected, and less energy are coupled to other ports). Others measured results agree well with the simulated results in Fig. 6 (b).

Compared with the 5G MIMO antennas proposed in recent years [13-17] and some traditional 4-port MIMO antennas [21-23], our antenna has a better performance in impedance match (S_{ii}) and ports isolation (S_{ij}), and its size keeps at a satisfactory level, as shown in Table 2 and Table 3.

Table 2: Performance comparison with previously reported 5G MIMO antennas

Ref.	Number of Elements	S_{ij} (dB)	S_{ii} (dB)	Size (mm^2)
[13]	4	< -12	< -6	130*74
[14]	8	< -10	< -13	145*75
[15]	8	< -15	< -10	130*100
[16]	4	< -12	< -6	120*50
[17]	8	< -20	< -10	150*75
This work	4	< -20	< -10	50*50

Table 3: Performance comparison with traditional 4-port MIMO antennas

Ref.	Bandwidth (GHz)	S_{ij} (dB)	Size (mm^2)
[21]	0.68-0.72&1.75-2.45	< -12	150*250
[22]	7.25-10.25	< -19	45*45
[23]	1.45-2.25&3.71-4.71	< -23	263*263
This work	3.3-5.8	< -20	50*50

Measured and simulated radiation patterns of *E*-plane (xoy-plane) and *H*-plane (xoz-plane) are shown in Fig. 9. When measuring radiation patterns, we keep port 1 excited and other ports loaded with a 50-Ω load. In measurement of radiation patterns, the MIMO antenna is used as the receiver, and a horn antenna with working bandwidth of 3-5 GHz is used as the transmitter. The

horn antenna remains fixed, and the receiver antenna rotates 360° to obtain a pattern of one plane. The cross-polarization in patterns is measured after the horn antenna rotates 90°. At 3.5 GHz and 4.9 GHz, the *E*-plane radiation patterns of the antenna element are quasi-directional. That means with the orthogonal placement of the four elements, this MIMO antenna can nearly cover all directions in *E*-plane. The co-polarization radiation patterns are quasi-omnidirectional in *H*-plane, and there are high-level of cross-polarization, but this won't affect the MIMO antenna's performance because the propagation paths in mobile wireless communication are generally multipath in diversity reception.

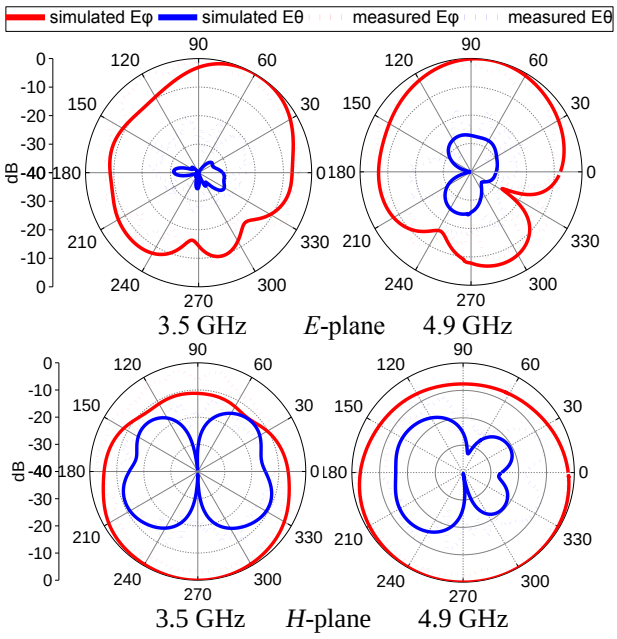

Fig. 9. Measured and simulated radiation patterns of *E*-plane and *H*-plane.

Another important parameter to evaluate the property of MIMO antenna is the envelope correlation coefficient (ECC). It's used to describe how much the communication channels are isolated or correlated with each other [4]. A low ECC means a good isolation between ports as well as high channel capacities. It can be calculated by the formula mentioned in [24] and [25]:

$$ECC_{ij} = \frac{\left|S_{ii}^{*}S_{ij} + S_{ji}^{*}S_{jj}\right|^{2}}{\left(1-\left|S_{ii}\right|^{2}-\left|S_{ji}\right|^{2}\right)\left(1-\left|S_{jj}\right|^{2}-\left|S_{ij}\right|^{2}\right)\eta_{rad,i}\eta_{rad,j}}, \quad (1)$$

the S-parameters and radiation efficiency η of antenna are involved in (1). As it shows in Fig. 10 the ECC of this MIMO antenna is less than 0.01 within the band, which means this antenna is competent for diversity reception/transmission in the MIMO channels. The simulated peak gains and total efficiency of the MIMO antenna are also respectively given in Fig. 11, within the range of 3-6 GHz (0.5 GHz/step): the peak gains can reach 5.0 dBi at 5 GHz and 2.5 dBi at 3.5 GHz; the total efficiency ranges within 51% - 79%.

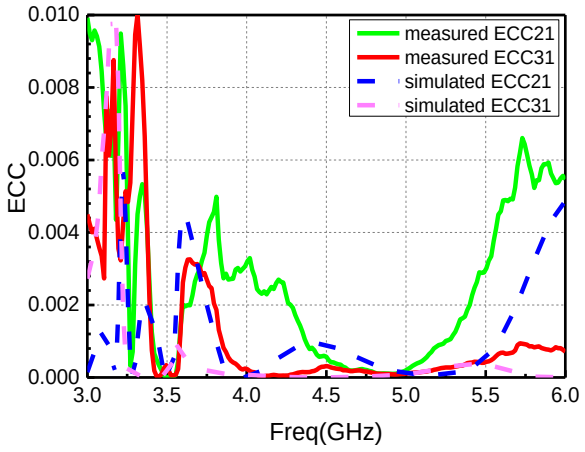

Fig. 10. Measured and simulated ECC.

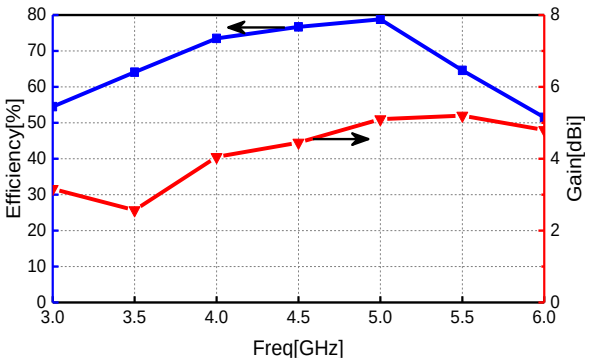

Fig. 11. Simulated peak gains and total efficiency.

B. Calculated channel capacity and CDF

Channel capacity means the maximum information transmission rate of this system, it's an important index to evaluate the quality of MIMO system and its unit is bps/Hz. The calculation of channel capacity is generally given by:

$$C = \log_2 \det(\mathbf{I}_N + \frac{\rho}{N_T}\mathbf{H}\mathbf{H}^H). \quad (2)$$

$\mathbf{I}_N$ means the identity matrix, ρ is the average of the signal-to-noise ratio (SNR) at receiver, N_T is the number of antenna elements at transmitter, $\mathbf{H}$ denotes the channel matrix and H represents the Hermitian transpose of matrix.

In [26], Hiroyuki Arai et al. proposed a MIMO antenna that can be used for 5G indoor base station; they calculated and measured its channel performance in indoor environment. In their work, the signal

transmission path of indoor base station antenna to the target was generally line-of-sight (LOS) channel with Ricean fading environment. But for the mobile terminal antenna, the transmission path of the general signal is non-line-of-sight (NLOS). In this case, the signal transmission path follows the Rayleigh fading distribution, such as the channel model established by Yong-ling Ban et al. in [27] used to calculate the channel capacity of mobile MIMO antenna. In order to calculate the capacity of the MIMO channel in this paper, we assume that two identical MIMO antennas as the receiver and transmitter with Rayleigh fading channel environment. Given the channel model in [28] as following:

$$\mathbf{H}=\mathbf{R}_{\mathrm{Rx}}^{1/2}\mathbf{H}_{\mathrm{w}}\mathbf{R}_{\mathrm{Tx}}^{1/2}, \tag{3}$$

where $\mathbf{R}_{\mathrm{Tx}}$ is the correlation matrix indicating the correlation between the transmitting antennas. Similarly, $\mathbf{R}_{\mathrm{Rx}}$ is the correlation matrix indicating the correlation between the receiving antennas. $\mathbf{H}_{\mathrm{w}}$ is the channel gain matrix with i.i.d. (independent identically distributed) Rayleigh fading. Referred from [28], $\mathbf{R}_{\mathrm{Tx}}$ and $\mathbf{R}_{\mathrm{Rx}}$ can be approximately expressed by:

$$\mathbf{R}_{\mathrm{Tx}}=\mathbf{I}-\mathbf{S}_{\mathrm{Tx}}^{\mathrm{H}}\mathbf{S}_{\mathrm{Tx}}, \tag{4}$$

$$\mathbf{R}_{\mathrm{Rx}}=\mathbf{I}-\mathbf{S}_{\mathrm{Rx}}^{\mathrm{H}}\mathbf{S}_{\mathrm{Rx}}, \tag{5}$$

where $\mathbf{S}_{\mathrm{Rx}}$ and $\mathbf{S}_{\mathrm{Tx}}$ are S-matrix of receiving and transmitting antennas respectively. Thus, (2) can be expressed as:

$$C=\log_2\det\left(\mathbf{I}_{N_{\mathrm{Rx}}}+\frac{\rho}{N_{\mathrm{Tx}}}\mathbf{R}_{\mathrm{Rx}}^{1/2}\mathbf{H}_{\mathrm{w}}\mathbf{R}_{\mathrm{Tx}}\mathbf{H}_{\mathrm{w}}^{\mathrm{H}}\mathbf{R}_{\mathrm{Rx}}^{\mathrm{H}/2}\right), \tag{6}$$

in our channel model, N_{Tx}=N_{Rx}=4, if the SNR is high enough, then formula (6) could be approximated as:

$$C\approx\log_2\det\left(\frac{\rho}{N_{\mathrm{Tx}}}\mathbf{H}_{\mathrm{w}}\mathbf{H}_{\mathrm{w}}^{\mathrm{H}}\right)+\log_2\det\left(\mathbf{R}_{\mathrm{Rx}}\right)+\log_2\det\left(\mathbf{R}_{\mathrm{Tx}}\right). \tag{7}$$

Since in our channel model the SNR is not as high as to be negligible, so we used formula (6) to calculate the channel capacity of the MIMO system composed of two MIMO antennas. Figure 12 shows the results of calculated channel capacity changing with SNR at different frequencies and gives the i.i.d. channel capacity as a comparison. It can be seen the MIMO channel performs best at 5.0 GHz while worst at 4.5 GHz. It's worth noting that at 5.0 GHz, the capacity is very close to the capacity of the i.i.d. channel.

However, if there are data transmission links in the channel, the communication interruptions are likely occurred. That is, the probability receiver cannot receive information correctly, and the cumulative distribution function (CDF) is used to describe it. Figure 13 shows the CDF of this MIMO channel under different SNR conditions at 3 GHz. It can be seen that the higher the SNR is, the lower the CDF and the probability of interruption are.

IV. CONCLUSION

A compact dual-band MIMO antenna is proposed in this paper, it works within the dual-band of 5G communications (sub-6 GHz): 3.3-3.6 GHz and 4.8-5.0 GHz. The antenna has an excellent overall performance. Its -10 dB-bandwidth can cover 3.3-5.8 GHz and the isolation between the ports can keep higher than 20 dB. The simulated results agree well with measured results and the antenna's ECC, peak gain, radiation patterns and total efficiency are given in the paper as well. The calculated channel capacity is close to the i.i.d. channel when antenna works at 5.0 GHz and the probability of communication interruption could be small when the SNR is high enough. But there are still some drawbacks on this MIMO antenna: the radiation pattern of single element cannot cover the entire *E*-plane and can't receive/radiate signals in some specific directions; its total efficiency is not very ideal, only 60% in some frequency bands.

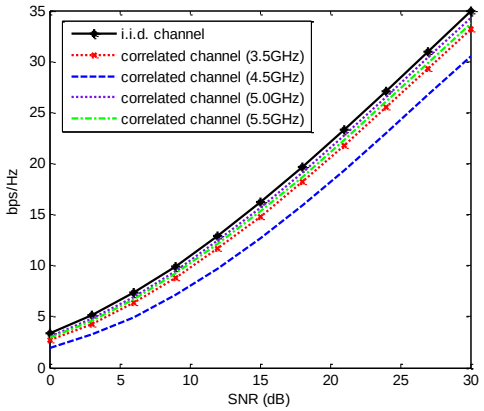

Fig. 12. Calculated channel capacity.

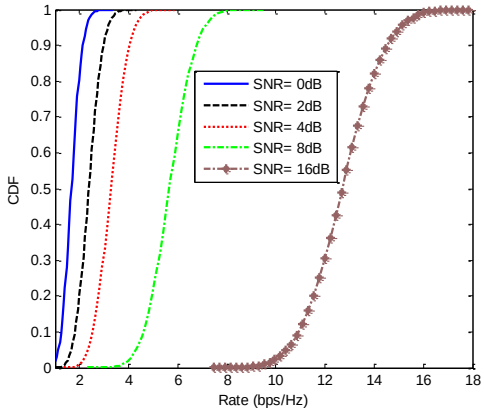

Fig. 13. Cumulative distribution function (CDF) of MIMO channel at 3 GHz.

ACKNOWLEDGMENT

This work was supported by the National Natural

Science Foundation of China (61701448, 61671415 and 61601414), and the Fundamental Research Funds for the Central Universities (CUC18A007-1 and CUC2019B091).

REFERENCES

[1] A. J. Paulraj, D. A. Gore, R. U. Nabar, and H. Bolcskei, "An overview of MIMO communications - A key to gigabit wireless," in *Proceedings of the IEEE*, vol. 92, no. 2, pp. 198-218, Feb. 2004.

[2] X.-L. Liu, Z.-D. Wang, Y.-Z. Yin, J. Ren, and J.-J. Wu, "A compact ultra-wideband MIMO antenna using QSCA for high isolation," in *IEEE Antennas and Wireless Propagation Letters*, vol. 13, pp. 1497-1500, 2014.

[3] J. Deng, J. Li, L. Zhao, and L. Guo, "A dual-band inverted-F MIMO antenna with enhanced isolation for WLAN applications," in *IEEE Antennas and Wireless Propagation Letters*, vol. 16, pp. 2270-2273, 2017.

[4] C. Luo, J. Hong, and L. Zhong, "Isolation enhancement of a very compact UWB-MIMO slot antenna with two defected ground structures," in *IEEE Antennas and Wireless Propagation Letters*, vol. 14, pp. 1766-1769, 2015.

[5] L. Kang, H. Li, X. Wang, and X. Shi, "Compact offset microstrip-fed MIMO antenna for band-notched UWB applications," in *IEEE Antennas and Wireless Propagation Letters*, vol. 14, pp. 1754-1757, 2015.

[6] S. Zhang and G. F. Pedersen, "Mutual coupling reduction for UWB MIMO antennas with a wideband neutralization line," in *IEEE Antennas and Wireless Propagation Letters*, vol. 15, pp. 166-169, 2016.

[7] F. Yang and Y. Rahmat-Samii, "Microstrip antennas integrated with electromagnetic band-gap (EBG) structures: a low mutual coupling design for array applications," in *IEEE Transactions on Antennas and Propagation*, vol. 51, no. 10, pp. 2936-2946, Oct. 2003.

[8] S. Ghosh, T. Tran, and T. Le-Ngoc, "A dual-layer EBG-based miniaturized patch multi-antenna structure," *2011 IEEE International Symposium on Antennas and Propagation (APSURSI)*, Spokane, WA, pp. 1828-1831, 2011.

[9] X. Tan, W. Wang, Y. Wu, Y. Liu, and A. A. Kishk, "Enhancing isolation in dual-band meander-line multiple antenna by employing split EBG structure," in *IEEE Transactions on Antennas and Propagation*, vol. 67, no. 4, pp. 2769-2774, Apr. 2019.

[10] M. Al-Hasan, I. B. Mabrouk, E. R. F. Almajali, M. Nedil, and T. A. Denidni, "Hybrid isolator for mutual-coupling reduction in millimeter-wave MIMO antenna systems," in *IEEE Access*, vol. 7, pp. 58466-58474, 2019.

[11] P. Qin, Y. J. Guo, and C. Liang, "Effect of antenna polarization diversity on MIMO system capacity," in *IEEE Antennas and Wireless Propagation Letters*, vol. 9, pp. 1092-1095, 2010.

[12] L. Dong, H. Choo, R. W. Heath, and Hao Ling, "Simulation of MIMO channel capacity with antenna polarization diversity," in *IEEE Transactions on Wireless Communications*, vol. 4, no. 4, pp. 1869-1873, July 2005.

[13] W. Zhang, Z. Weng, and L. Wang, "Design of a dual-band MIMO antenna for 5G smartphone application," *2018 International Workshop on Antenna Technology (iWAT)*, Nanjing, pp. 1-3, 2018.

[14] K. Yan, P. Yang, F. Yang, L. Y. Zeng, and S. Huang, "Eight-antenna array in the 5G smartphone for the dual-band MIMO system," *2018 IEEE International Symposium on Antennas and Propagation & USNC/URSI National Radio Science Meeting*, Boston, MA, pp. 41-42, 2018.

[15] Y. Li, H. Zou, M. Wang, M. Peng, and G. Yang, "Eight-element MIMO antenna array for 5G/Sub-6GHz indoor micro wireless access points," *2018 International Workshop on Antenna Technology (iWAT)*, Nanjing, pp. 1-4, 2018.

[16] I. Dioum, K. Diallo, M. M. Khouma, I. Diop, L. Sane, and A. Ngom, "Miniature MIMO antennas for 5G mobile terminals," *2018 6th International Conference on Multimedia Computing and Systems (ICMCS)*, Rabat, pp. 1-6, 2018.

[17] A. Zhao and Z. Ren, "Size reduction of self-isolated MIMO antenna system for 5G mobile phone applications," in *IEEE Antennas and Wireless Propagation Letters*, vol. 18, no. 1, pp. 152-156, Jan. 2019.

[18] A. A. Qureshi, M. U. Afzal, T. Tauqeer, and M. A. Tarar, "Performance analysis of FR-4 substrate for high frequency microstrip antennas," *2011 China-Japan Joint Microwave Conference*, Hangzhou, pp. 1-4, 2011.

[19] M. Liang, F. Zhang, G. Zhang, and Q. Li, "Broadband dual-polarized antennas with high port isolation for portable devices," *Proceedings of 2014 3rd Asia-Pacific Conference on Antennas and Propagation*, Harbin, pp. 359-362, 2014.

[20] B. P. Chacko, G. Augustin, and T. A. Denidni, "Compact uni-planar antenna with polarization diversity for UWB applicaton in portable devices," *2014 IEEE Antennas and Propagation Society International Symposium (APSURSI)*, Memphis, TN, pp. 1809-1810, 2014.

[21] Y. Lu, Y. Chan, H. Li, Y. Lin, S. Lo, and G. C. Chuang, "Design and system performances of a dual-band 4-Port MIMO antenna for LTE applications," *2011 IEEE International Symposium*

on Antennas and Propagation (APSURSI), Spokane, WA, pp. 2227-2230, 2011.

[22] J. Motohashi and M. Yamamoto, "A wideband 4-port MIMO antenna using leaf-shaped notch antennas," *2016 International Symposium on Antennas and Propagation (ISAP)*, Okinawa, pp. 1070-1071, 2016.

[23] S. S. Jehangir, A. Hassan, and M. S. Sharawi, "A 4-element dual wideband circular Yagi MIMO antenna system with loop excitation," *2016 IEEE International Symposium on Antennas and Propagation (APSURSI)*, Fajardo, pp. 69-70, 2016.

[24] P. Hallbjorner, "The significance of radiation efficiencies when using S-parameters to calculate the received signal correlation from two antennas," in *IEEE Antennas and Wireless Propagation Letters*, vol. 4, pp. 97-99, 2005.

[25] S. Blanch, J. Romeu, and I. Corbella, "Exact representation of antenna system diversity performance from input parameter description," in *Electronics Letters*, vol. 39, no. 9, pp. 705-707, 1 May 2003.

[26] B. Rohani, K. Takahashi, H. Arai, Y. Kimura, and T. Ihara, "Improving channel capacity in indoor 4×4 MIMO base station utilizing small bi-directional antenna," in *IEEE Transactions on Antennas and Propagation*, vol. 66, no. 1, pp. 393-400, Jan. 2018.

[27] Y. Ban, C. Li, C. Sim, G. Wu, and K. Wong, "4G/5G multiple antennas for future multi-mode smartphone applications," in *IEEE Access*, vol. 4, pp. 2981-2988, 2016.

[28] N. Honma, H. Sato, K. Ogawa, and Y. Tsunekawa, "Accuracy of MIMO channel capacity equation based only on S -parameters of MIMO antenna," in *IEEE Antennas and Wireless Propagation Letters*, vol. 14, pp. 1250-1253, 2015.